Waves over Soft Muds: A Two-Layer Fluid Model

ROBERT A. DALRYMPLE[1]

Department of Civil Engineering, University of Delaware, Newark, DE 19711

PHILIP L.-F. LIU

Department of Environmental Engineering, Cornell University, Ithaca, NY 14853

(Manuscript received 6 April 1978, in final form 9 June 1978)

ABSTRACT

The problem of water waves propagating over a mud bottom, characterized as a laminar viscous fluid, is treated in several ways. First, two complete models are present, each valid for different lower (mud) layer depths, and second, a boundary layer model is presented as an appendix for the case where the lower layer is thick with respect to the boundary layer.

These models are compared to the shallow water model and experimental results of Gade (1957, 1958) and agree well. The results show that extremely high wave attenuation rates are possible when the thickness of the lower layer is the same order as the internal boundary layer thickness and when the lower layer is thick.

1. Introduction

Classical water wave theories for use in offshore design have had the theoretical drawback of assuming a rigid, nonporous bottom overlain by an inviscid fluid. In most offshore areas, however, the bottom material interacts with the wave field, usually resulting in an attenuation of the wave height due to bottom friction, percolation losses and viscous damping within the sediments. These interactive effects are manifested also by changes in wavelength and water particle motions as well as changes in the location of the interface between the fluid and the bottom sediments.

The damping of the surface waves can be considerable; in fact, Gade (1958) notes that there is a location in the Gulf of Mexico, known as the Mud Hole, where the attenuation of waves due to the mud bottom is so great that fishing boats use it as an emergency harbor during storms. Silvester (1974, p. 196) describes a location where waves are attenuated after propagating only several wavelengths.

To an offshore designer, the implication of the bottom-induced effects on the waves are reduced wave loads on a structure, wave refraction and wave scattering due to pockets of sediments (Lassiter, 1972), and significant soil motions around marine pipelines.

The type of bottom material over which the waves are propagating in this paper is assumed to be similar to a viscous fluid, characterized by a viscosity and a density greater than the overlying fluid. This type of bottom has been treated previously by Gade (1957, 1958) (for shallow water). Other types of bottoms have also been studied previously: elastic—Mallard and Dalrymple (1977); porous—Hunt (1959) and Liu (1973) among many; poro-elastic—Yamamoto (1977) and Liu and Dalrymple (1978).

The theories developed herein are for a linear water wave propagating in a two-layer viscous fluid system. The height of the surface wave is specified and the forced interfacial wave is determined, as well as the attenuation rate of the wave.

The first models, denoted the complete models, are developed to be valid for any depth upper layer and both deep and shallow lower fluid layers, thus extending Gade's results to deeper water. These models also include the viscous effects in the upper layer for completeness, although the damping effects there are quite small when compared to the lower, more viscous layer. The second model, presented in Appendix C, is a boundary layer approach, which is analytically simpler, and yields explicit solutions for the wave damping when the thickness of the lower layer is greater than the boundary layer thickness developed by the fluid motion.

The results of models are compared to the shallow water experimental results obtained by Gade (1957) and agree quite well; in fact, in most cases in

[1] Also affiliated with the College of Marine Studies and the Institute for Mathematical Sciences.

0022-3670/78/1121-1131$05.50

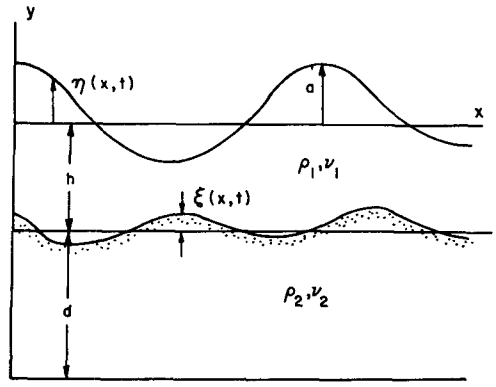

FIG. 1. Schematic figure for the two-layer fluid model.

shallow water, the present complete models are identical to Gade's model. In deeper water, a second example is presented for the complete models to show the effects of larger water depths.

An interesting result of the experiments and the complete models is that there is a maximum attenuation rate which occurs when the thickness of the lower layer is about 30% greater than the corresponding boundary layer thickness $(\sigma/2\nu_2)^{1/2}$, where σ is the wave angular frequency and ν_2 the viscosity of the lower fluid. For these cases, the attenuation of wave height can be very large; for example, for Gade's tests, a wave will be reduced to one-tenth of its original height after propagating only 2.6 wavelengths!

2. Complete model theory

The wave under consideration is propagating in the x direction in water of depth h over a viscous layer of thickness d. See Fig. 1 for notation. The viscosity is of importance in both regions but is of prime concern near the fluid boundaries. The free surface displacement is denoted by $\eta(x,t)$ and the interface between the two fluids is $\xi(x,t)$. These displacements are given by $\eta = ae^{i(kx-\sigma t)}$ and $\xi = be^{i(kx-\sigma t)}$. The amplitude a is assumed known as well as the frequency $\sigma = 2\pi/T$, where T is the wave period.

The equations of motion for the fluid motions are the laminar Navier-Stokes equations for an incompressible fluid, which have been linearized by neglecting the convective accelerations:

$$\frac{\partial \hat{u}_i}{\partial t} = -\frac{1}{\rho_i}\frac{\partial \hat{P}_i}{\partial x} + \nu_i\left(\frac{\partial^2 \hat{u}_i}{\partial x^2} + \frac{\partial^2 \hat{u}_i}{\partial y^2}\right), \quad (1)$$

$$\frac{\partial \hat{v}_i}{\partial t} = -\frac{1}{\rho_i}\frac{\partial \hat{P}_i}{\partial y} + \nu_i\left(\frac{\partial^2 \hat{v}_i}{\partial x^2} + \frac{\partial^2 \hat{v}_i}{\partial y^2}\right), \quad (2)$$

with the subscripts $i = 1, 2$ indicating the upper and lower layers, respectively, x, y denote the horizontal and vertical axes situated at the mean water level, and $\hat{P}_i$ is the dynamic pressure defined as $\hat{P}_i = \hat{P}_i^t + \rho_i g y + P_i^0$, where P_i^t denotes the total pressure and

$$P_i^0 = \begin{cases} 0, & \text{for } i = 1 \\ (\rho_2 - \rho_1)gh, & \text{for } i = 2. \end{cases} \quad (3)$$

The conservation of mass (continuity) equation is

$$\frac{\partial \hat{u}_i}{\partial x} + \frac{\partial \hat{v}_i}{\partial y} = 0. \quad (4)$$

The solutions to these equations for $\hat{u}_i$, $\hat{v}_i$, $\hat{P}_i$ are assumed separable and periodic in time and the x direction. They are expressed as

$$\left.\begin{aligned} \hat{u}_i(x,y;t) &= u_i(y)e^{i(kx-\sigma t)} \\ \hat{v}_i(x,y;t) &= v_i(y)e^{i(kx-\sigma t)} \\ \hat{P}_i(x,y;t) &= P_i(y)e^{i(kx-\sigma t)} \end{aligned}\right\}, \quad (5)$$

where $k = 2\pi/L$ is the wavenumber. From the continuity equation (4),

$$u_i = iv_i'/k, \quad (6)$$

where the prime indicates differentiation with respect to y. Introducing this expression for u_i into the horizontal momentum equation (1) yields an expression for P_i, i.e.,

$$P_i = (\rho_i\nu_i/k^2)[v_i''' - v_i'(k^2 - i\sigma\nu_i^{-1})]. \quad (7)$$

Substituting P_i into the vertical momentum equation (2) yields the governing differential equation for v_i:

$$v_i^{(iv)} - (2k^2 - i\sigma\nu^{-1})v_i'' + k^2(k^2 - i\sigma\nu_i^{-1})v_i = 0$$

or

$$v_i^{(iv)} - (k^2 + \lambda_i^2)v_i'' + k^2\lambda_i^2 v_i = 0, \quad (8)$$

where

$$\lambda_i^2 = k^2 - i\sigma\nu_i^{-1}. \quad (9)$$

These equations, for the upper and lower fluids, may be solved readily, but first it simplifies the problem to examine the influence of the λ_i. For most problems ν_i is quite small with respect to k by several orders of magnitude. Consequently, the λ_i are quite large and in fact represent the viscosity-dominated flow in the vicinity of boundaries. Away from the boundaries, i.e., outside any boundary layers, the viscous terms are negligible. Therefore, solutions will be chosen which contain viscous terms near the boundary (terms preceded by C, D, G, H, below), but they will be neglected far from the boundaries. Appendix B will discuss the case where the lower layer is of the same order as the boundary layers, which is the case used for comparison to Gade's experimental results, and Appendix C presents a boundary layer model for the lower fluid alone, which yields an explicit analytical solution.

The assumed solutions here are

$$v_1(y) = A \sinh k(h + y) + B \cosh k(h + y) + Ce^{\lambda_1 y} + De^{-\lambda_1(h+y)}, \quad (10)$$

$$v_2(y) = E \sinh k(h + y + d) + F \cosh k(h + y + d) + Ge^{\lambda_2(h+y)} + He^{-\lambda_2(h+d+y)}, \quad (11)$$

and the $u_i(y)$ are given by (6).

With the assumed solutions containing eight unknown constants (A–H) and the interface displacement, also unknown, nine boundary conditions must be specified; plus, as in the case of an irrotational wave, one additional condition is required to provide a dispersion relationship relating k to σ.

At the fixed bottom, $y = -(h + d)$, the velocities in both the horizontal and vertical directions must be zero, i.e.,

$$\left.\begin{aligned} \hat{v}_2 &= 0 \\ \hat{u}_2 &= 0 \quad \text{at} \quad y = -(h + d) \end{aligned}\right\} \quad (12)$$

or

$$\left.\begin{aligned} F + H &= 0 \\ kE - \lambda_2 H &= 0 \quad \text{from (6) and (11)} \end{aligned}\right\}. \quad (13)$$

Note that the G term is considered to be zero this far from the interface between the two fluids.

At the interface, denoted by $\xi = be^{i(kx-\sigma t)}$, with b being *a priori* unknown, a kinematic condition is specified which, due to the assumed linearity of the problem, is applied at $y = -h$.

$$\partial\xi/\partial t = \hat{v}_i \quad \text{on} \quad y = -h$$

or

$$-i\sigma b = B + D. \quad (14)$$

The vertical and horizontal velocities must also be continuous

$$\hat{v}_1 = \hat{v}_2,$$

$$\hat{u}_1 = \hat{u}_2 \quad \text{on} \quad y = -h,$$

or

$$B + D = E \sinh kd + F \cosh kd + G, \quad (15)$$

$$Ak - \lambda_1 D = Ek \cosh kd + Fk \sinh kd + G\lambda_2. \quad (16)$$

The normal and tangential stresses will also be continuous across the interface. The normal stress is written as $\sigma_{yy}(x,y) = \hat{P}_i^t - 2\rho_i\nu_i(\partial\hat{v}_i/\partial y)$. To evaluate σ_{yy} at the interface, a Taylor Series expansion is used about $y = -h$. To first order in wave amplitude,

$$\sigma_{yy}(x, -h + \xi) = \hat{P}_i^t(x, -h) - 2\rho_i\nu_i \frac{\partial\hat{v}_i}{\partial y} + \frac{\partial\hat{P}_i^t}{\partial y}(x, -h)\xi.$$

The continuity of σ_{yy} and τ_{xy} across the interface, where $\tau_{xy} = \mu(\partial\hat{u}/\partial y + \partial\hat{v}/\partial x)$ is then written as

$$\hat{P}_1 - 2\rho_1\nu_1 \frac{\partial\hat{v}_1}{\partial y} - \rho_1 g\xi = \hat{P}_2 - 2\rho_2\nu_2 \frac{\partial\hat{v}_2}{\partial y} - \rho_2 g\xi, \quad (17)$$

$$\rho_1\nu_1\left(\frac{\partial\hat{u}_1}{\partial y} + \frac{\partial\hat{v}_1}{\partial x}\right) = \rho_2\nu_2\left(\frac{\partial\hat{u}_2}{\partial y} + \frac{\partial\hat{v}_2}{\partial x}\right) \quad \text{on} \quad y = -h, \quad (18)$$

or

$$M_1 A + 2\rho_1\nu_1\lambda_1 D = M_2[E \cosh kd + F \sinh kd] - 2\rho_2\nu_2\lambda_2 G - (\rho_2 - \rho_1)gb, \quad (19)$$

where

$$M_i = \left(\frac{i\rho_i\sigma}{k} - 2\rho_i\nu_i k\right), \quad (20)$$

$$\rho_1\nu_1[2k^2B + (\lambda_1^2 + k^2)D] = \rho_2\nu_2[2k^2E \sinh kd + 2k^2F \cosh kd + (\lambda_2^2 + k^2)G]. \quad (21)$$

At the free surface, a kinematic boundary condition, requiring the surface particles to follow the surface, is applied as well as the imposition of zero normal and tangential stresses:

$$\left.\begin{aligned} \frac{\partial\eta}{\partial t} &= \hat{v}_1, && \text{on} \quad y = \eta, \\ \hat{P}_1^t - 2\rho_1\nu_1 \frac{\partial\hat{v}_1}{\partial y} &= 0, && \text{on} \quad y = \eta \\ \rho_1\nu_1\left(\frac{\partial\hat{u}_1}{\partial y} + \frac{\partial\hat{v}_1}{\partial x}\right) &= 0, && \text{on} \quad y = \eta \end{aligned}\right\},$$

or after a first-order Taylor Series expansion about $y = 0$,

$$-i\sigma a = A \sinh kh + B \cosh kh + C, \quad (22)$$

$$M_1(A \cosh kh + B \sinh kh) - \rho_1 ga - 2\rho_1\nu_1\lambda_1 C = 0, \quad (23)$$

$$2Ak^2 \sinh kh + 2Bk^2 \cosh kh + (\lambda^2 + k^2)C = 0. \quad (24)$$

Ten conditions have now been prescribed for eight unknowns, the interface displacement b, and k which are all complex. The solution may be found by substitution and iteration as is discussed in Appendix A.

3. Comparison with experiment

The resulting models were applied to model tests performed by Gade (1957) in a wave tank with a length of 1.83 m, a depth of 0.3 m and a width

of 0.152 m. The two-fluid systems consisted of kerosine in the upper layer and a water-sugar solution in the lower layer. The wave system was created by a wave maker at one end and wave absorbers at the other end were used to reduce the reflection. His test conditions were based on fixing the depth of the upper layer at $h = 3.81 \times 10^{-2}$ m and varying d, the lower layer depth. Further, $\sigma = 4.488\ s^{-1}$, $\rho_1 = 859.3\ kg\ m^{-3}$, $\rho_2 = 1504\ kg\ m^{-3}$, $\nu_1 = 2.42 \times 10^{-6}\ m^2\ s^{-1}$, $\nu_2 = 2.60 \times 10^{-3}\ m^3\ s^{-1}$.

The experimental measurements included rates of wave height decay along the tank, and the maximum horizontal displacements at the corresponding points on the interface and the surface. Photographs were taken of the tank for the measurements of wavelength and surface and interfacial profiles. Floating chips of cork or wood, measured against a fixed scale, were utilized for these measurements.

Errors in the experiment noted by Gade were occasioned by 1) the frictional resistance of the side walls, 2) the irregularity of the generated wave profile and its deviation from a sinusoidal profile, and 3) reflection from the end wall, particularly at the two observations obtained at $(\sigma/2\nu_2)^{1/2}d = 1.4, 1.68$.

Fig. 2 shows the model test results for wave damping in terms of k_i, the imaginary part of the wavenumber. The relationship between the wave amplitude a and k_i is

$$a = a_0 e^{-k_i x},$$

where a_0 is the reference amplitude at the origin. The figure clearly shows that there is a maximum of the wave damping with respect to the lower depth thickness. This maximum occurs due to the nature of the work done in the lower layer by the upper layer. This work consists of two parts, the pressure in the upper fluid working on the vertical velocity of the interface, $P_1^t \hat{v}_2$, and the shear stress working on the interface, $\tau_{xy}\hat{u}_1$. In most cases, i.e., when the lower layer is of reasonable thickness with respect to the boundary layer scale, $(\sigma/2\nu_2)^{1/2}d > 1$, the first of these is of most importance, and its efficiency depends on the phase difference between P_1^t and $\hat{v}_2(=\partial\xi/\partial t)$ being a maximum when they are in phase. As the depth of the lower layer increases, $\hat{v}_2$ changes in phase monotonically from $-\pi$ to $-\pi/2$ and the work therefore increases up to a maximum and then decreases.

It is interesting to note that the complete model and Gade's theory agree quite well, except at the low values of $(\sigma/2\nu_2)^{1/2}d$, which is the ratio of the thickness of the lower layer to the boundary layer thickness (when the damping in the upper layer is rela-

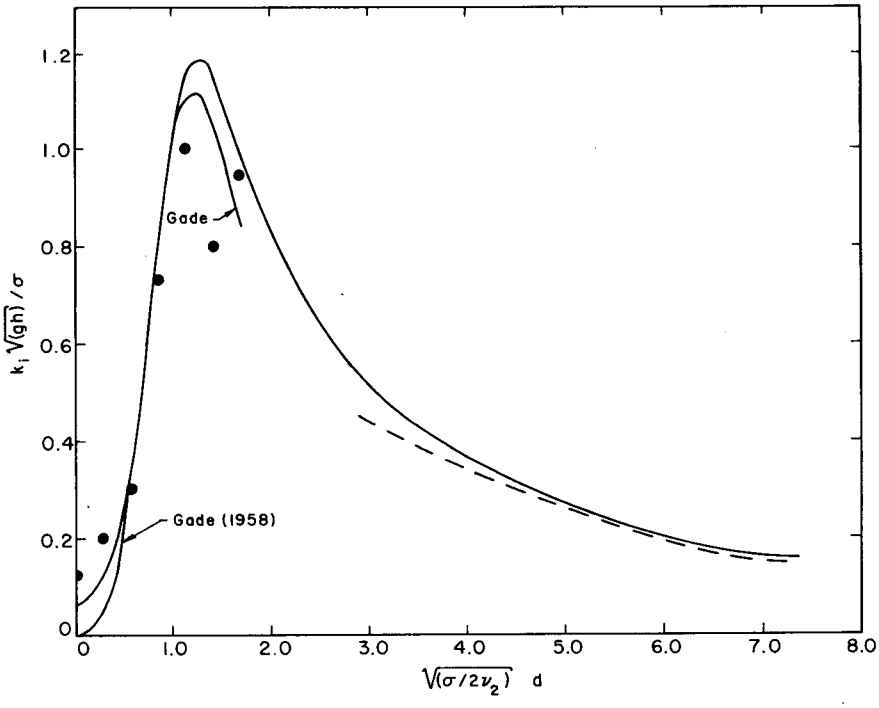

FIG. 2. Comparison of dimensionless damping coefficient k_i (the complex part of the wavenumber) versus dimensionless lower layer depth d as calculated by the complete models. The data points correspond to Gade's (1957) experiment and the dashed line is the result of the boundary layer model developed in Appendix C. The characteristics of the fluids and wave are $T = 1.4$ s, $h = 3.81 \times 10^{-2}$ m, $\nu_1 = 2.42 \times 10^{-6}\ m^2\ s^{-1}$, $\nu_2 = 2.6 \times 10^{-3}\ m^2\ s^{-1}$, $\rho_1 = 859.3\ kg\ m^{-3}$, $\rho_2 = 1504\ kg\ m^{-3}$.

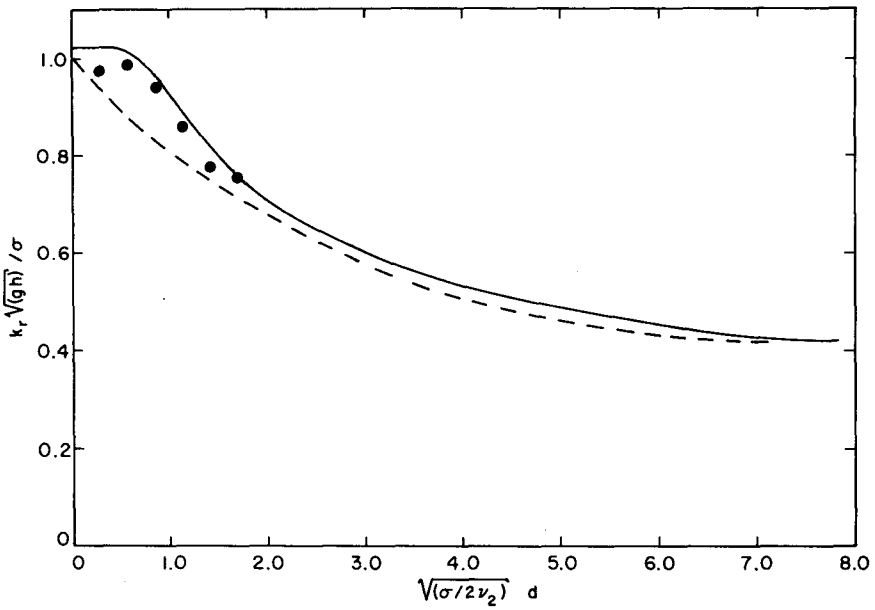

FIG. 3. Comparison of dimensionless wavenumber k_r (real part of the wavenumber) versus the dimensionless lower layer depth d. Data from Gade (1957). The dashed line is the boundary layer model.

tively important) and for high values of this parameter, which begin to exceed the shallow water conditions imposed by Gade.

In Fig. 3, the wavelength of the wave system (inversely proportional to k_r) is plotted. There is little disagreement with Gade's theory (not shown). As can be seen, the real part k_r of the wavenumber decreases with the depth of the lower layer, as expected from shoaling considerations. The agreement with the experimental results again in this case is quite good.

In Fig. 4, the relative amplitude of the interfacial wave for Gade's test parameters is shown, in terms of magnitude and phase. As the lower fluid layer becomes thicker, d increasing, the magnitude of the interfacial wave increases (as stated before, the upper fluid's ability to do work on the lower layer becomes more efficient) and its phase with respect to the free surface profile monotonically decreases. At great depths in the lower layer, the interfacial wave becomes more in phase with the free surface wave, lagging it only slightly. The

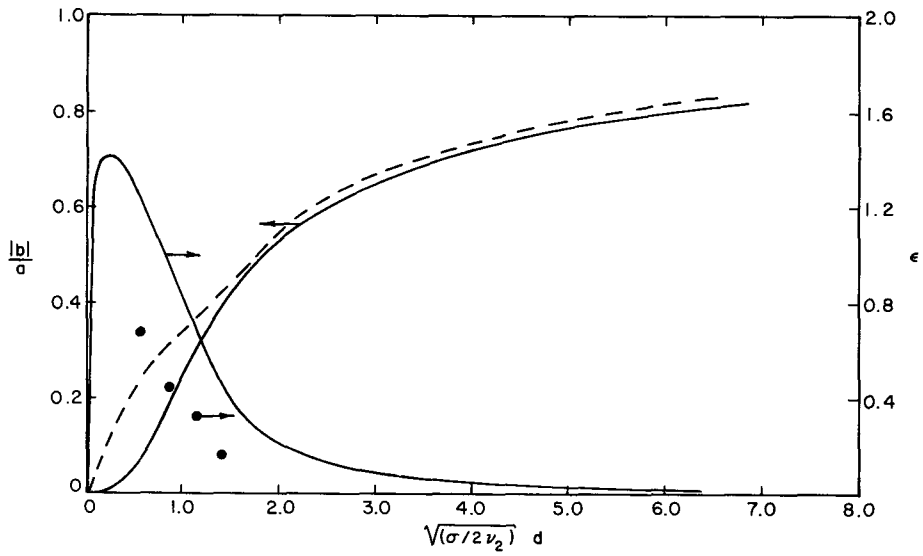

FIG. 4. Ratio of interfacial to surface wave amplitude and phase difference plotted against dimensionless lower layer depth d. Note that Gade's data points are for phase.

errors in phase between measured and predicted (by either model) are the worst here by about a factor of 2.

The velocity profiles and dimensionless pressure, $\hat{P}_i - P_i^0$ are plotted in Fig. 5 for $(\sigma/2\nu_2)^{1/2}d = 1.119$. Due to the shallowness of the upper layer, the $\hat{u}_1$ and $\hat{P}_1$ do not vary significantly with depth, while $\hat{v}_1$ is almost linear with depth. In the lower layer where the boundary layers are of the same magnitude as the thickness d, there is a strong variation of $\hat{u}_2$ with depth. The phase shifts ϵ over the depth are also shown, and it is indicated for the horizontal velocity, for example, that the maximum velocity in the upper layer precedes the crest arrival by a small amount, while in the lower layer the velocity lags significantly, almost by $\pi/4$.

4. Case II: Deeper water

A second example, more corresponding to actual field conditions, was carried out for the following data: $h = 4$ m, $\sigma = 1.2566$ s^{-1}, $\rho_1 = 1028$ kg m^{-3}, $\rho_2 = 1800$ kg m^{-3}, $\nu_1 = 2.6 \times 10^{-6}$ m^2 s^{-1}, $\nu_2 = 0.1$ m^2 s^{-1}. In Fig. 6 the dimensionless damping is shown for various values of d and again a peak is evident. The thickness of the lower layer corresponding to this case is about 0.6 m. In Gade's tests the peak damping occurred at $(\sigma/2\nu_2)^{1/2}d \approx 1.3$, while in this case $(\sigma/2\nu_2)^{1/2}d \approx 1.5$, leading to the general conclusion, supported by other cases, that where the depth of the lower fluid is about 10–50% more than the boundary layer thickness parameter, $(\sigma/2\nu_2)^{-1/2}$, then peak damping will occur. This evidence of peak damping occurring for a fixed ratio of $(\sigma/2\nu_2)^{1/2}d$ has design implications for the use of bottom-mounted breakwaters, filled with viscous fluids (see, e.g., Weigel, 1964; Frederiksen, 1971).

In Fig. 7, the real part k_r of the wavenumber is plotted, showing the significant decrease in wavelength for very shallow lower layer depths when compared to the same wave over a fixed bottom, where $k_r(gh/\sigma)^{1/2} = 1.0$.

For actual cases, when the boundary layer in the upper layer is negligible, the relevant dimensionless numbers characterizing the model are d/h, ρ_1/ρ_2, $\sigma^2 h/g$ and $(\sigma/2\nu_2)^{1/2}d$. For the previous example, d was varied while h had been fixed at 4 m. In Fig. 8, ν_2 alone has been varied for various ratios of d/h, to illustrate the influence of viscosity. Clearly, the thicker the lower layer [with $(\sigma/2\nu_2)^{1/2}d$ of O(1)], the greater the damping. For $d/h = 0.5$, or $d = 2$ m, peak damping occurs at $(\sigma/2\nu_2)^{1/2}d = 1.3$, at a value about 3.8 times greater than for the case above. (The wave height will be reduced to one-tenth its original height within 7.7 wave lengths, or 225.5 m.)

5. Conclusions

Two models [for small and large values of $(\sigma/2\nu_2)^{1/2}d$] of water waves propagating over a very viscous fluid, such as might characterize bottom muds have been developed, which extend the analysis of Gade (1957, 1958) to deeper water conditions and includes the viscosity in the upper fluid. A boundary layer model valid for large values of $(\sigma/2\nu_2)^{1/2}d$ has also been developed and has been shown to agree well with the complete model. One model (for shallow water) was applied to Gade's model tests and agrees with the data quite well for wave damping and wavelength, whereas the phase between the interface and the free surface displacements are in error by about a factor of 2, as was Gade's analysis.

For values of $(\sigma/2\nu_2)^{1/2}d$ between 1.1–1.5, there is a peak value of the damping coefficient k_i.

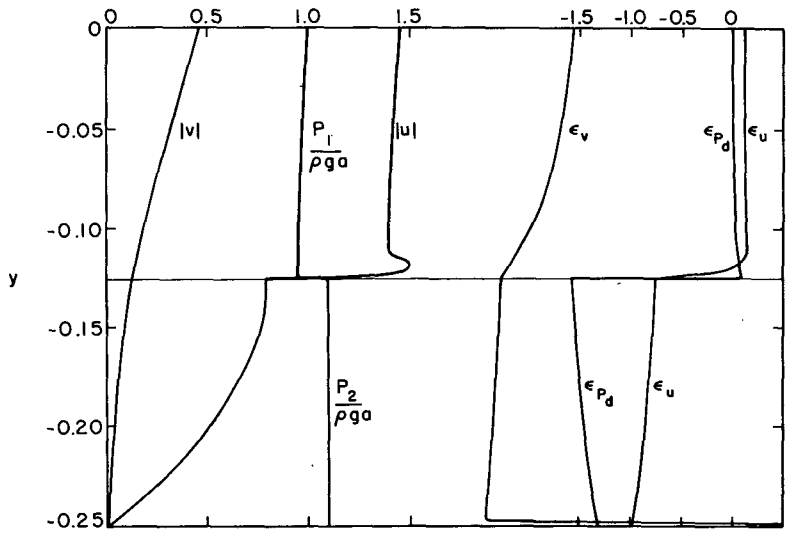

FIG. 5. Magnitude of the velocities (cm s^{-1}) and dimensionless pressure and the associated phases (with respect to wave profile) plotted for $(\sigma/2\nu_2)^{1/2}d = 1.119$ and Gade's test parameters.

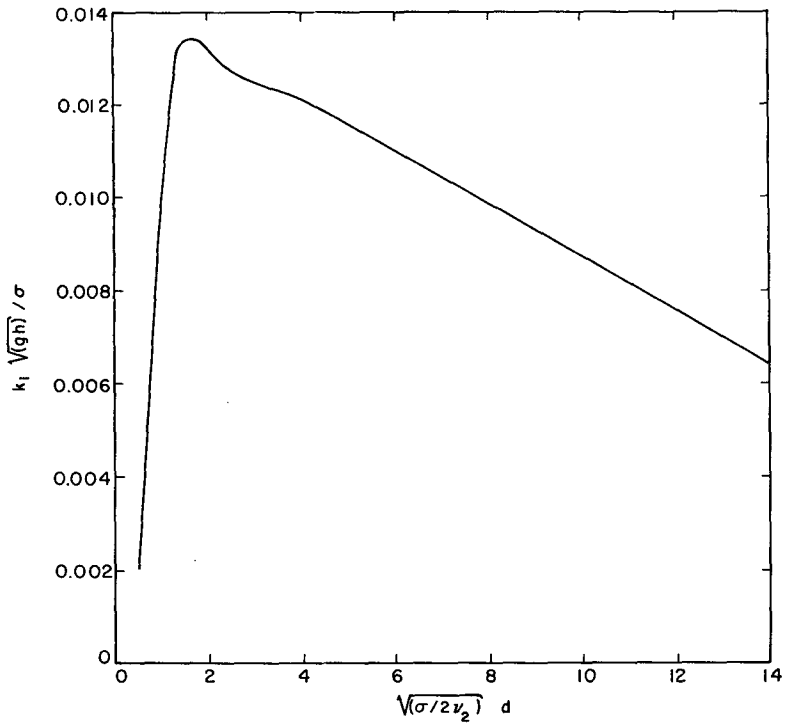

FIG. 6. Dimensionless damping coefficient for the Case II wave as a function of dimensionless lower layer depth. The characteristics of the fluids and waves are $T = 5$ s, $h = 4$ m, $\nu_1 = 2.6 \times 10^{-6}$ m^2 s^{-1}, $\nu_2 = 0.1$ m^2 s^{-1}, $\rho_1 = 1028$ kg m^{-3}, $\rho_2 = 1800$ kg m^{-3}.

Further, as d/h increases the damping increases also. This damping can be significant, reducing wave heights drastically over a distance of several wavelengths.

From Fig. 2, where Gade's model and the present model agree well, despite Gade's neglect of interfacial shear stress in upper fluid, the conclusion is drawn that the principal method of energy transfer

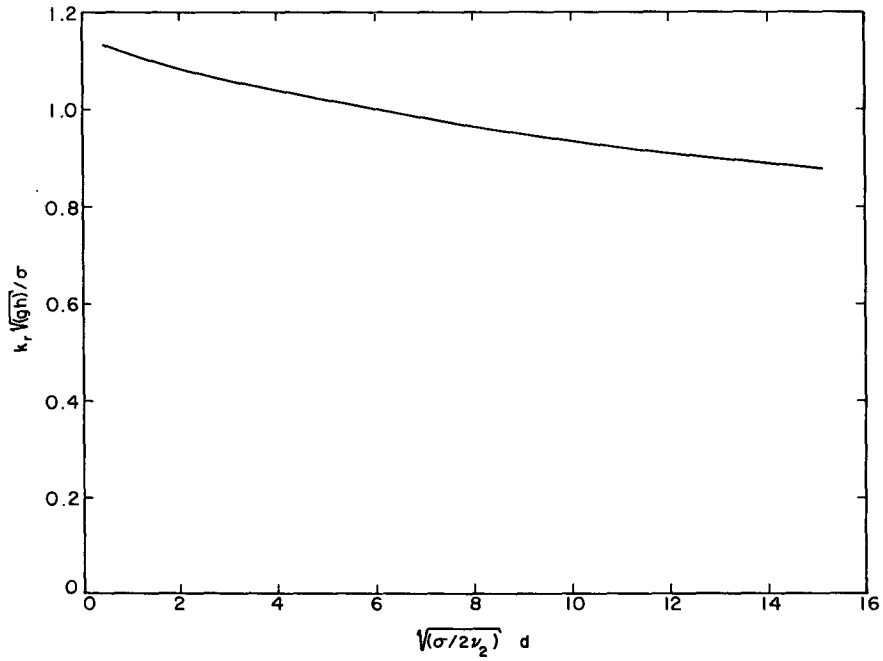

FIG. 7. Dimensionless wavenumber k_r versus the dimensionless lower layer depth for the Case II wave.

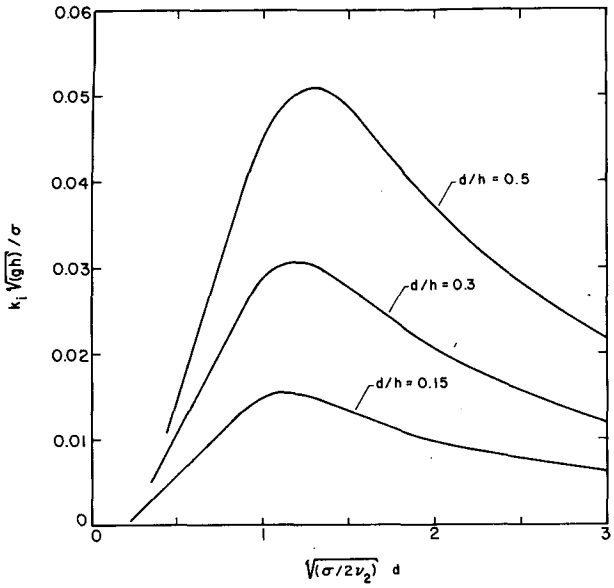

FIG. 8. Dimensionless damping coefficient for the Case II wave as a function of dimensionless lower layer viscosity ν_2. Note that peak damping occurs at $(\sigma/2\nu_2)^{1/2}d = 1.1$–$1.3$ for these cases. The characteristics of the fluids and wave are $T = 5$ s, $h = 4$ m, $\nu_1 = 2.6 \times 10^{-6}$ m^2 s^{-1}, $\rho_1 = 1028$ kg m^{-3}, $\rho_2 = 1800$ kg m^{-3}.

to the lower layer is the pressure of the surface wave working on the lower fluid.

Acknowledgments. The authors would like to thank Professor R. O. Reid for supplying the Gade thesis to us. This research was sponsored, in part, by the New York Sea Grant Institute, under a grant from the NOAA Office of Sea Grant, U. S. Department of Commerce, and through a contract with the Office of Naval Research, Geography Programs, Arlington, VA 22217.

APPENDIX A

Solution Techniques

The solution to the two-layer viscous fluid model follows from the use of the ten boundary conditions which were derived for the nine complex unknowns $(A$–$H,b)$ and the unknown complex wavenumber k.

The brute force solution technique would be to reduce one of the two inhomogeneous equations (22) and (23) to a homogeneous form using the other. This would then leave a 9×9 homogeneous matrix for the nine unknowns. In order for a homogeneous matrix equation to have solutions the coefficient matrix would have to be singular (cf. Wylie, 1960). Therefore an iterative technique based on, say, the secant method, would be used to find the value of k for which the determinant is zero; then the matrix equation would be solved for the nine unknowns. This solution would be correct to within an arbitrary constant, which would then be eliminated by use of the remaining homogeneous equation. This technique, while feasible, has the drawback that a large determinant must be evaluated numerous times.

A more laborious technique is to solve the matrix equation directly. This follows by making the following substitutions which reduces the 10×9 matrix to a 4×3.

Eqs. (13), (14), (15), (16), as well as $2k^2$ times Eqs. (22)–(24), yield six equations for F, E, b, B, A, C, respectively, which depend on D, G and H, with the exception of $C(= -2\nu ak^2)$. Substitution of these expressions into the 10×9 matrix yields a 4×3 matrix:

$$(c_{ij}) \cdot \begin{pmatrix} D \\ G \\ H \end{pmatrix} = \begin{pmatrix} \dfrac{-M_1 ka}{\rho} \\ +\rho ga \\ \dfrac{-4\rho\nu^2 ak^2\lambda_1}{M_1} \\ 0 \end{pmatrix}, \quad i = 1, 3, \quad j = 1, 4, \tag{A1}$$

where the c_{ij} are

$$\begin{pmatrix} \left(\dfrac{\lambda_1}{k}\sinh kh - \cosh kh\right) & \left(\dfrac{\lambda_2}{k}\sinh kh + \cosh kh\right) & (-S\sinh kh - Q\cosh kh) \\ \left(\dfrac{\lambda_1}{k}\cosh kh - \sinh kh\right) & \left(\dfrac{\lambda_2}{k}\cosh kh + \sinh kh\right) & -S\cosh kh - Q\sinh kh \\ \rho\nu_1(\lambda_1^2 - k^2) & (2\rho_1\nu_1k^2 - \rho_2\nu_2(\lambda_2^2 + k^2)) & (2\rho_2\nu_2k^2 - 2\rho_1\nu_1k^2) \\ \dfrac{\lambda_1}{k}M_1 + 2\rho\nu_1\lambda_1 & \left(\dfrac{\lambda_2}{k}M_1 + 2\rho_2\nu_2\lambda_2 + \dfrac{i}{\sigma}(\rho_s - \rho)g\right) & (M_2 - M_1)S - \dfrac{i}{\sigma}(\rho_2 - \rho_1)gQ \end{pmatrix} \tag{A2}$$

and where $S = \sinh kd - (\lambda_2/k)\cosh kd$, $Q = \cosh kd - (\lambda_2/k)\sinh kd$, and M_1, M_2 are defined in Eq. (20). The c_{31} and c_{41} may be simplified to $-i\rho\sigma$ and $i\rho\sigma(\lambda_1/k^2)$, respectively. Therefore, c_{41} may be reduced to zero by subtracting $\lambda_1/k^2 \cdot$(row 3) from row 4.

Therefore row 4 states

$$G = -\frac{c_{43}H}{c_{42}}.$$

By back substituting into rows 3 and 2, D and G are found in terms of k and a; of which a is assumed known. Therefore only the value of k remains to be found and the remaining row (row 1) is used for this purpose. This is done by a complex secant method which is used iteratively until a complex k is found to solve row 1 in an acceptable manner (10^{-9} was used). The problem is therefore solved.

In practice the accuracy of the complex arithmetic for the coefficients is of paramount importance and double precision is recommended for computational purposes.

APPENDIX B

Thin Lower Layer

In order to compare the results of the model to Gade's results and to make the technique generally applicable, it is necessary to solve the case for which the lower layer is of the same order of magnitude as the boundary layers within the region, i.e., $d = O(\sigma/2\nu_2)^{1/2}$.

The forms of the solution in the lower layer are modified

$$v_2 = E\sinh k(h + d + y) + F\cosh k(h + d + y) + G\sinh\lambda_2(h + d + y) + H\cosh\lambda_2(h + d + y). \quad \text{(B1)}$$

The u_2 is still given by (6) and P_2, (7). The solution technique follows exactly as before.

APPENDIX C

Boundary Layer Approximation

When the parameters

$$\epsilon_i = \frac{\sigma^2}{g}\left(\frac{\nu_i}{\sigma}\right)^{1/2}, \quad i = 1, 2,$$

are small, the flow motion is essentially irrotational except near boundaries where viscous boundary layers are of thickness the order of $(\nu_i/\sigma)^{1/2}$, $i = 1, 2$. Energy dissipation takes place in 1) the essentially inviscid core, 2) the free-surface boundary layer, 3) the boundary layer near the solid bottom, and 4) the boundary layers near the interface. If the free surface is uncontaminated, these contributions are, respectively, proportional to ν_i $(i = 1, 2)$, $\nu_2^{3/2}$ and $\nu_i^{1/2}$ $(i = 1, 2)$ (see Mei and Liu, 1973, and Johns, 1968). Therefore, the boundary layers near the solid bottom and the interface are most significant.

Following the approach taken by Liu (1973), one can split the velocity field into a potential part $\nabla\phi_i$ and a rotational part $\mathbf{U}_i$, $i = 1, 2$. The rotational velocity is significant only near the solid bottom and the interface. The linearized Navier-Stokes equations [Eqs. (1) and (2)] and the continuity equation [Eq. (4)] can be rewritten in the following forms:

$$\nabla^2\phi_1 = 0, \quad -h < y < 0, \quad \text{(C1)}$$

$$\nabla^2\phi_2 = 0, \quad -(h + d) < y < -h, \quad \text{(C2)}$$

$$\frac{\partial \mathbf{U}_i}{\partial t} = \nu_i\nabla^2\mathbf{U}_i, \quad \text{(C3)}$$

$$\hat{P}_i = -\rho_i\frac{\partial\phi_i}{\partial t}. \quad \text{(C4)}$$

The potential velocity can be readily solved, which is subject to the linearized boundary conditions as follows:

1) Free-surface boundary conditions ($y = 0$)

$$\frac{\partial\eta}{\partial t} = \frac{\partial\phi_1}{\partial y}, \quad \text{(C5)}$$

$$\frac{\partial\phi_1}{\partial t} + g\eta = 0. \quad \text{(C6)}$$

2) Interfacial boundary conditions ($y = -h$)

$$\frac{\partial\xi}{\partial t} = \frac{\partial\phi_1}{\partial y}, \quad \text{(C7)}$$

$$\frac{\partial\phi_1}{\partial y} = \frac{\partial\phi_2}{\partial y}, \quad \text{(C8)}$$

$$\rho_1\frac{\partial\phi}{\partial t} + \rho_1 g\xi = \rho_2\frac{\partial\phi_2}{\partial t} + \rho_2 g\xi. \quad \text{(C9)}$$

3) Solid bottom boundary condition ($y = -h - d$)

$$\frac{\partial\phi_2}{\partial y} = 0, \quad \text{(C10)}$$

where the free-surface profile $\eta = ae^{i(kx-\sigma t)}$. After some algebra, the potential flow solutions can be obtained as follows:

$$\phi_1 = -(iga/\sigma)\sinh ky[(\sigma^2/gk) + \coth ky]e^{i(kx-\sigma t)}, \quad \text{(C11)}$$

$$\phi_2 = -(iga/\sigma)(\cosh kh/\sinh kd)\cosh[k(y + h + d)] \times [(\sigma^2/gk) - \tanh kh]e^{i(kx-\sigma t)}, \quad \text{(C12)}$$

$$\xi = (gka/\sigma^2)\cosh kh \times [(\sigma^2/gk) - \tanh kh]e^{i(kx-\sigma t)}. \quad \text{(C13)}$$

The dispersion relation reads

$$\sigma^2/gk = [-l - (l^2 - 4mn)^{1/2}]/2m, \quad \text{(C14)}$$

$$l = -(\rho_2/\rho_1)\tanh k(h + d) \times (1 + \tanh kd \tanh kh), \quad \text{(C15)}$$

$$m = (\rho_2/\rho_1) + \tanh kh \tanh kd, \quad \text{(C16)}$$

$$n = [(\rho_2/\rho_1) - 1]\tanh kd \tanh kh. \quad \text{(C17)}$$

It is easy to show that the following special cases are true:

(i) $\rho_2 = \rho_1$

$$\sigma^2/gk = \tanh k(h + d) \quad \text{(C18)}$$

(ii) $d = 0$

$$\sigma^2/gk = \tanh kh \quad \text{(C19)}$$

(iii) $kd \ll 1$ and $kh \ll 1$

$$\sigma^2/gk = \tfrac{1}{2}k \times \{d + h + [(d - h)^2 + 4(\rho_1/\rho_2)hd]^{1/2}\}. \quad \text{(C20)}$$

The boundary layer solutions near the interface must satisfy the governing equation

$$\frac{\partial U_i}{\partial t} = \nu_i \frac{\partial^2 U_i}{\partial y^2}, \quad i = 1, 2, \quad \text{(C21)}$$

and the boundary conditions

$$\frac{\partial \phi_1}{\partial x} + U_1 = \frac{\partial \phi_2}{\partial x} + U_2, \quad y = -h, \quad \text{(C22)}$$

$$\rho_1\nu_1 \frac{\partial U_1}{\partial y} = \rho_2\nu_2 \frac{\partial U_2}{\partial y}, \quad y = -h. \quad \text{(C23)}$$

Here U_i, $i = 1, 2$, denotes the rotational velocity components in the direction of wave propagation in the upper and lower layer, respectively. The corresponding vertical rotational velocity components, which are one order of magnitude smaller than the horizontal velocity components, can be obtained by integrating the continuity equation (see, Mei and Liu, 1973). The rotational velocity diminishes outside the boundary layers.

Introducing the solution forms

$$U_1 = C_1 \times \exp[-(1 + i)(\sigma/2\nu_i)^{1/2}(y + h)]e^{i(kx-\sigma t)}, \quad \text{(C23)}$$

$$U_2 = C_2 \times \exp[(1 + i)(\sigma/2\nu_2)^{1/2}(y + h)]e^{i(kx-\sigma t)}, \quad \text{(C24)}$$

which satisfy the governing equation [Eq. (C21)] and substituting them into Eqs. (C22) and (C23) yield

$$C_1 = -\frac{gka}{\sigma \sinh kh} \frac{[(\rho_2/\rho_1)(\nu_2/\nu_1)^{1/2}]}{[1 + (\rho_2/\rho_1)(\nu_2/\nu_1)^{1/2}]} \times \{(\sigma^2/gk) - \tfrac{1}{2}\sinh 2kh[\coth kh + \coth kd] \times [(\sigma^2/gk) - \tanh kh]\}, \quad \text{(C25)}$$

$$C_2 = -(\rho_2/\rho_1)(\nu_1/\nu_2)^{1/2}C_1. \quad \text{(C26)}$$

Similarly, near the solid bottom a rotational velocity must be added in order to satisfy the no-slip condition,

$$\frac{\partial \phi_2}{\partial x} + U_3 = 0, \quad y = -(h + d), \quad \text{(C27)}$$

where U_3 represents the horizontal rotational velocity component inside the boundary layer. Assuming a solution form

$$U_3 = C_3 \times \exp[-(1 + i)(\sigma/2\nu_2)^{1/2}(y + h + d)]e^{i(kx-\sigma t)} \quad \text{(C28)}$$

and applying the boundary condition [Eq. (C27)] results in

$$C_3 = -\frac{gka}{\sigma}\frac{\cosh kh}{\sinh kd}\left(\frac{\sigma^2}{gk} - \tanh kh\right). \quad \text{(C29)}$$

To estimate the wave damping, one can follow the wave energy front and write the total rate of change of time-average wave energy density (Ippen, 1966) as

$$\frac{d\bar{E}}{dt} = C_g \frac{d\bar{E}}{dx} = -\bar{P}_d, \quad \text{(C30)}$$

where $C_g = d\omega/dk$ is the group velocity, $\bar{E}$ the time-average wave energy density and $\bar{P}_d$ the average rate of energy dissipation.

The time-average wave energy density can be written as

$$\bar{E} = 2\overline{\int_{-(h+d)}^{-h+\xi} \rho_2 g y dy} + 2\overline{\int_{-h+\xi}^{\eta} \rho_1 g y dy} = \rho_1 g\overline{\eta^2} + (\rho_2 - \rho_1)g\overline{\xi^2}. \quad \text{(C31)}$$

Equal partition of potential energy and kinetic energy has been employed. The overbar denotes the time-average over one wave period. The energy dissipation occurs in the boundary layers, thus

$$\bar{P}_d = \rho_1\nu_1 \int_{-h}^{"\infty"} \overline{\left(\frac{\partial U_1}{\partial y}\right)^2} dy + \rho_2\nu_2 \int_{"-\infty"}^{-h} \overline{\left(\frac{\partial U_2}{\partial y}\right)^2} dy + \rho_2\nu_2 \int_{-(h+d)}^{"\infty"} \overline{\left(\frac{\partial U_3}{\partial y}\right)^2} dy, \quad \text{(C32)}$$

where "$\pm\infty$" indicates the location outside of the boundary layers.

Substitutions of Eqs. (C13), (C23), (C24), (C28), (C31), and (C32) into Eq. (C30) result in

$$k_i = \frac{(\sigma\nu_1)^{1/2}[C_1^2 + (\rho_2/\rho_1)(\nu_2/\nu_1)^{1/2}(C_2^2 + C_3^2)]}{2gC_g a^2\{1 + [(\rho_2/\rho_1) - 1](kg/\sigma^2)^2 \cosh^2 kh[(\sigma^2/gk) - \tanh kh]^2\}}, \tag{C33}$$

where C_1, C_2 and C_3 are given in Eqs. (C25), (C26) and (C29), respectively. For the shallow water situations, $kh \ll 1$ and $kd \ll 1$, the damping coefficient can be written as

$$k_i = \frac{(2d)^{-2}(gk/\sigma^2)(\nu_1/\sigma)^{1/2}\{[k(d + h) - (\sigma^2/gk)]^2 + [1 + (\rho_2/\rho_1)(\nu_2/\nu_1)^{1/2}][(\sigma^2/gk) - kh]^2\}}{[1 + (\rho_1/\rho_2)(\nu_1/\nu_2)^{1/2}]\{1 + [(\rho_2/\rho_1) - 1][1 - (gk/\sigma^2)kh]^2\}}. \tag{C34}$$

The corresponding dispersion relation is given in Eq. (C20).

REFERENCES

Frederiksen, H. D., 1971: Wave attenuation by fluid filled bags. *J. Waterways, Harbors and Coastal Eng. Div., ASCE*, **97**, No. WW1, 73–90.

Gade, H. G., 1957: Effects of a non-rigid, impermeable bottom on plane surface waves in shallow water. Ph.D. thesis, Texas A & M University, 35 pp.

——, 1958: Effects of a non-rigid, impermeable bottom on plane surface waves in shallow water. *J. Mar. Res.*, **16**, 61–82.

Hunt, J. N., 1959: On the damping of gravity waves propagated over a permeable surface. *J. Geophys. Res.*, **64**, 437–442.

Ippen, A. T., Ed., 1966: *Estuary and Coastline Hydrodynamics*. McGraw-Hill, 744 pp.

Johns, B., 1968: A boundary layer method for the determination of viscous damping of small amplitude gravity waves. *Quart. J. Mech. Appl. Math.*, **21**, 93–103.

Lassiter, J., 1972: The propagation of water waves over sediment pockets, Ph.D. thesis, MIT, 54 pp.

Liu, P. L.-F., 1973: Damping of water waves over porous bed. *J. Hyd. Div., ASCE*, **99**, 2263–2271.

——, and R. A. Dalrymple, 1978: Water waves propagated over elastic porous seabeds. Submitted to *J. Waterways, Port, Coastal and Ocean Div., ASCE*.

Mallard, W. W., and R. A. Dalrymple, 1977: Water waves propagating over a deformable bottom. *Proc. Offshore Tech. Conf.*, OTC 2895.

Mei, C. C., and P. L.-F. Liu, 1973: The damping of surface gravity waves in a bounded fluid. *J. Fluid Mech.*, **59**, 239–256.

Silvester, R., 1974: *Coastal Engineering*, Vol. 1, Elsevier, 457 pp.

Wiegel, R. L., 1964: *Oceanographical Engineering*. Prentice-Hall, 532 pp.

Wylie, C. R., 1960: *Advanced Engineering Mathematics*, 2nd ed. McGraw-Hill 696 pp.

Yamamoto, T., 1977: Wave-induced instability of seabeds. *Proc. ASCE Symp. Coastal Sediments*, Charleston, 898–913.